IET Science, Measurement & Technology

Research Article

IET Journals
The Institution of Engineering and Technology

Separation of adjacent interharmonics using maximum energy retrieving algorithm

ISSN 1751-8822
Received on 2nd June 2015
Revised on 15th September 2015
Accepted on 18th September 2015
doi: 10.1049/iet-smt.2015.0115
www.ietdl.org

Hsiung Cheng Lin ✉

Department of Electronic Engineering, National Chin-Yi University of Technology, Taiwan
✉ *E-mail: hclin@ncut.edu.tw*

Abstract: It is known that flickers and interharmonics have an inherent relationship, and the magnitude of a voltage can fluctuate as the signal contains interharmonics. In particular, flicker or modulation will occur when the interharmonic is close to a harmonic (or fundamental) frequency. Current spectrum separation approaches can detect harmonics and main interharmonics effectively, but they may not be applicable for the situation of adjacent interharmonics from either divergence effect, sensitive spectral leakage or other drawbacks. For this reason, this study develops a strategy of maximum energy retrieving (MER) method to distinguish and identify those interharmonics which are adjacent to fundamental or harmonics in power systems. Based on the appropriate selection of sampling window length using discrete Fourier transform (DFT), neighbouring dispersed energy can be collected to retrieve its original amplitude value. The frequency component can be thus determined simultaneously when the total collected energy reaches the maximum. The MER implementation can be converged within only several iteration loops where parallel DFT computation is required before the convergent process. The numerical example is used to verify the effectiveness of the proposed approach in term of reliability and accuracy.

1 Introduction

With increasing growth of power electronics system and periodical time-varying loads used in industry, it has caused the distortion of the ideal electric sine wave, producing a number of harmonics/interharmonics. Consequently, the quality of the electric power may be seriously deteriorated, and the apparatus connected to the electric net may be badly acted [1, 2]. Impacts of interharmonics are similar to those of harmonics such as filter overloading, light flicker, thermal effects, malfunctioning of remote control system, saturation of current transformers, subsynchronous oscillatoions, acoustic disturbance, overload of passive parallel filter, low-frequency oscillation in a mechanical system, voltage fluctuations, interference with control and protection signals, erroneous firing of thyristor apparatus, etc. These phenomenons may appear even under a low amplitude [3–7]. The interharmonic fluctuating magnitude is essentially a source of voltage flicker. If the magnitude is sufficiently large and the fluctuation frequency is located in a range of perceptible human eyes, a light flicker will occur. Currently, flicker monitoring/mitigation technique still needs improvement to handle interharmonic problems. The designing and evaluation of mitigation measures to reduce the flicker impact of interharmonics is therefore an indispensable task [8, 9].

Discrete Fourier transform (DFT) is the most popular tool to analyse harmonics. In fact, if the width of sampling window is not properly chosen, some negative aspects such as spectral leakage or picker fence effects will arise. For this reason, in the past many related approaches have been reported in the literature [10–15]. However, when the system fundamental frequency varies or harmonics/interharmonics are present in the measured waveforms, these approaches may suffer from low accuracy and less computational efficiency. Some studies are addressed to modify the FFT using windows and interpolations that can reduce the leakage, but it is unable to detect interharmonics near harmonics due to low spectrum resolution [16–18]. Therefore, the classical Hanning window is often recommended to replace the rectangular window [19]. Another techniques using time-domain or frequency-domain offer either computational efficiency or good solution accuracy. Nevertheless, their limits do not suggest as a definitive algorithms [20, 21]. Artificial neural networks are also applied in signal analysis. The initial parameters' setting, however, discourages their further applications [22, 23]. An algorithm that uses adjustable sampling frequency and correspondingly an adjustable window size was reported [24]. Its theory is based on the decimation and interpolation techniques on both harmonic and polyharmonic signals. Unfortunately, the mechanism would be collapsed when the size of the rectangular window is close to a multiple of the signal period. An exact calculation of harmonics/interharmonics using adaptive window width was also proposed [25]. The window width calculation uses an iterative optimisation procedure to search for the most suitable solution. For generic signal waveforms of unknown frequency, its iteration loop requires a larger initial value to avoid deceptively strong correlation. As a result, significantly longer computational time cannot be ignored in this case.

An efficient algorithm using the combination of Prony-based method and the downsampling technique for harmonics and interharmonics detection was proposed [26]. The selection of downsampling coefficient (alpha) and estimation order (K), however, relies on the measured signal considerably. The solution accuracy may be thus affected due to lack of an effectively convergent mechanism. The proposed sliding-window ESPRIT algorithm allows for accurate frequency estimation of interharmonic components [27]. It requires specifying the number of frequency components. This limitation sometimes leads to spurious components, line splitting and occasional failure. Although this disadvantage was overcome by the proposed Exact Model Order ESPRIT Technique using the RD plot, more computational time required may pose a difficulty delivered into a practical application [28]. Recently, a new method to separate and analyse harmonics and interharmonics based on the basis of single channel blind source separation was proposed. The orthogonal vector in its proposed model lacks an effectively convergent mechanism so that its implementation may not be convinced in reality [29]. Also, only distant interharmonics and harmonics such as 40, 50, 80, 175, 250 Hz can be separated successfully. Another proposed approach related to spectrum separation for detecting harmonics and main interharmonics was also reported [30]. Although this method can identify interharmonic component when the frequency difference between the harmonic and interharmonic is <5 Hz, the proposed model may collapse due to very sensitive

to spectral leakage. Another interesting method known as interpolated DFT was applied successfully in the parameters estimation of signals by reducing spectral leakage [31, 32]. One successful case study is for the estimation of frequency and amplitude using rectangular and Hanning windows in the periodic signals [31]. Moreover, it was widely used in the analysis of the exponential signal. However, this interpolation algorithm relies on the effective bits of the A/D conversion, on the position of the frequency component of the signal and on the mutual component interspacing along the frequency axis [32]. The interpolated DFT techniques were known as being focused on only some specific topics so that currently it is unsuitable to work out the problem of adjacent interharmonics.

IEEE Interharmonic Task Force has adopted IEC standard for interharmonic definition, measurement and limitation, it has two major limitations: (i) Interharmonic frequencies may not be found accurately under this standard due to the central frequency of interharmonics group defined as the group frequency. (ii) Those interharmonics close to fundamental or harmonics may not be detected properly [33]. Actually, many studies focused on interharmonic sources, impacts, measurement, limit values and mitigation can be found in the recent literature [34–46]. The research should be carried on in finding accurate interharmonic magnitude and frequency for adjacent harmonics/interharmonics [47].

2 Mathematical background on group-harmonic concept using DFT

The principle of Fourier analysis is to reconstruct a non-sinusoidal periodical waveform by a series sinusoidal component. Harmonic is defined as the component whose frequency is a multiple of fundamental. For a distorted waveform $i_s(t)$, if it is a continuous periodical signal and it satisfies Dirichlet condition, we can represent it as

$$i_s(t) = \sum_{n=-\infty}^{\infty} i_n \, e^{j2\pi ft} \tag{1}$$

where $i_n = 1/T \int_0^T i_s(t)\, e^{-j2\pi ft}\, dt$, and $T(=1/f)$ is the period. i_0 is the dc component.

The signal must be converted into a discrete form to be implemented in computer or microprocessor for Fourier analysis. DFT is then introduced as

$$i_s[n] = \sum_{k=0}^{N-1} I_s[k] W_N^{kn} \tag{2}$$

where

$$I_s[k] = \frac{1}{N} \sum_{n=0}^{N-1} i_s[n] W_N^{-kn}, \quad \text{and} \quad W_N = \exp(j2\pi/N).$$

Assume $i_s[n]$ is periodic with the period T. The Fourier fundamental angular frequency ($\Delta\omega$) can be defined as

$$\Delta\omega = \frac{2\pi}{T} \tag{3}$$

The waveform is sampled using $p(p>1)$ periods, and $\Delta\omega$ can be represented as

$$\Delta\omega = \frac{2\pi}{pT} = \frac{\omega_0}{p} \tag{4}$$

where $\omega_0 = 2\pi/T$.

Therefore, Fourier fundamental frequency (Δf) can be written as

$$\Delta f = \frac{1}{pT} = \frac{1}{pN_s T_s} = \frac{1}{NT_s} = \frac{f_s}{N} \tag{5}$$

where $N_s \triangleq N/p$ and $T_s \triangleq 1/f_s$. Note that the signal is sampled N points by sampling rate f_s, and the Fourier fundamental period is defined as the sampling time $T_f = N \cdot (1/f_s)$.

According to the Parseval relation, the power of the waveform, P, can be expressed in its discrete form [48, 49] as

$$P = \frac{1}{N} \sum_{n=0}^{N-1} i_s[n]^2 = \sum_{k=0}^{N-1} I_s[k]^2 \tag{6}$$

The power at the frequency f_k can be expressed as [48]

$$P[f_k] = I_s[k]^2 + I_s[N-k]^2 = 2I_s[k]^2 \tag{7}$$

where $k = 0, 1, 2, \ldots, N/2 - 1$.

Accordingly, the amplitude of mth harmonic at f_k is obtained as

$$A_m[f_k] = \sqrt{P[f_k]} = \sqrt{2} I_s[k] \tag{8}$$

where $m = 1, 2, \ldots, M$.

The power of the mth harmonic at f_k will disperse over around the f_k if the sampling window is not synchronised with the fundamental. Based on the grouping concept, all spilled power around the adjacent harmonics/interharmonics can be restored into a 'group power'

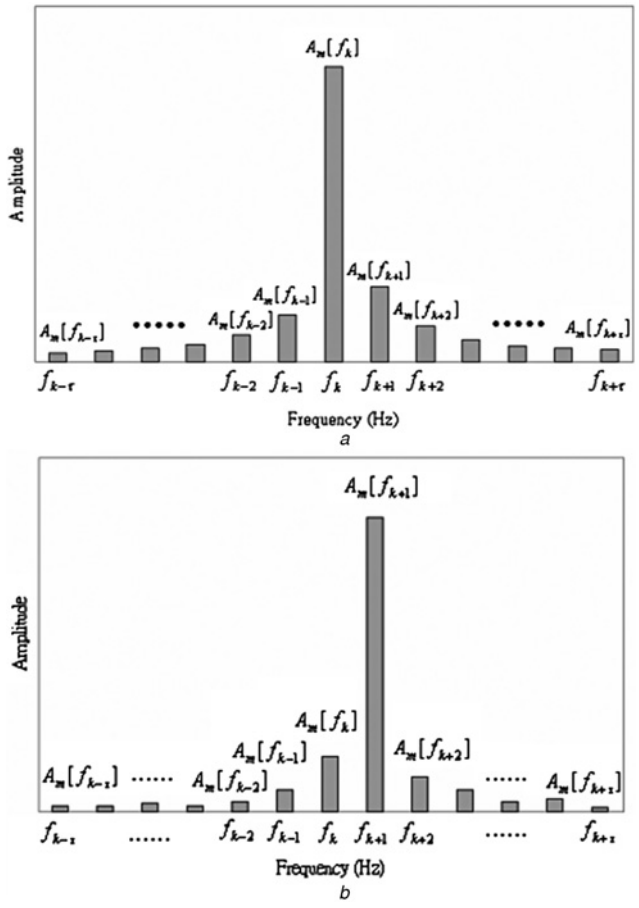

Fig. 1 *Relation between harmonic frequency and dispersed energy*
a Small frequency deviation
b Big frequency deviation

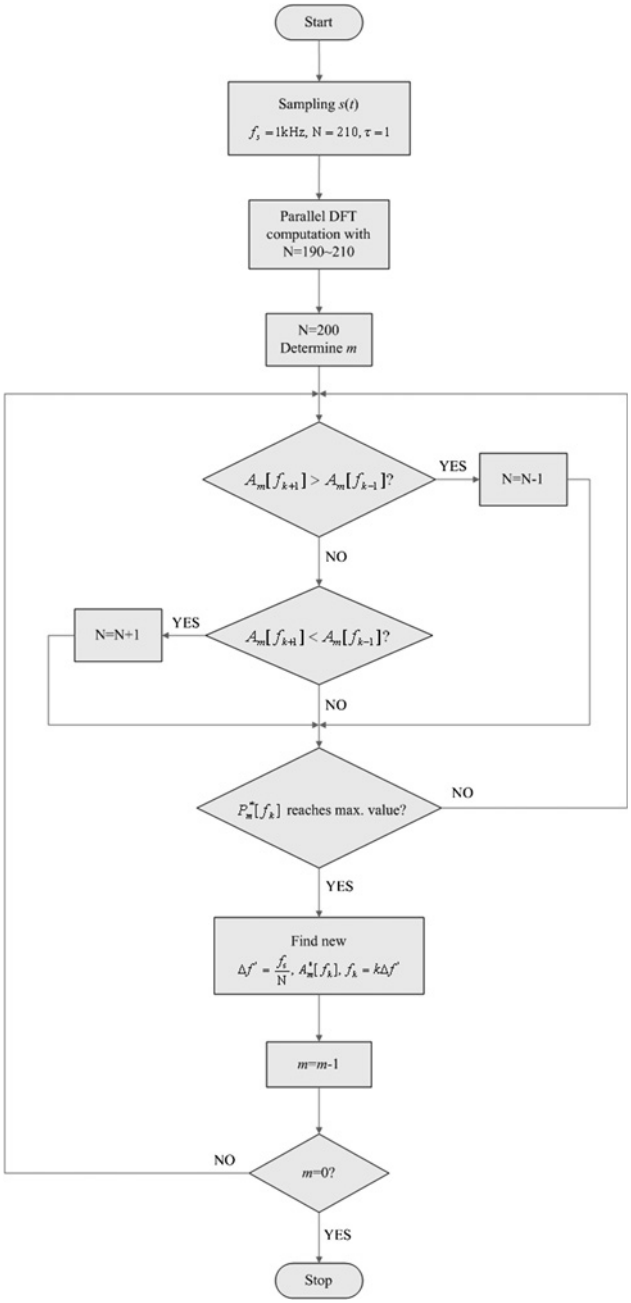

Fig. 2 *Flowchart of the proposed MER algorithm*

$(P_m^*[f_k])$ between $f_{k-\Delta k}$ and $f_{k+\Delta k}$ [45].

$$P_m^*[f_k] = \sum_{\Delta k=-\tau}^{+\tau} P_m[f_{k+\Delta k}] = \sum_{\Delta k=-\tau}^{+\tau} (A_m[f_{k+\Delta k}])^2 \quad (9)$$

where τ denotes the group bandwidth.

The true harmonic amplitude can be calculated as

$$A_m^*[f_k] = \sqrt{P_m^*[f_k]} \quad (10)$$

3 Proposed algorithm

Based on the empirical observation, the relation between harmonic frequency and dispersed energy can be induced and defined. Consider the following cases based on DFT analysis. Case 1: Fig. 1*a* reveals that the second larger magnitude $(A_m[f_{k+1}])$ at f_{k+1} is located at the right-hand side of the dominant frequency at f_k, where $A_m[f_k] > A_m[f_{k+1}]$. Generally, f_k may be wrongly interpreted as the dominant harmonic frequency. Actually, it is found that the true frequency known as an interharmonic should be equal to f_k plus the 'frequency deviation' (Δf_k) [40]. It is confirmed that higher $A_m[f_{k+1}]$ will introduce more amounts of deviation (Δf_k) from f_k. Similarly, Case 2 shows another situation in Fig. 1*b* that the second larger amplitude $(A_m[f_k])$ at f_k is located at the left-hand side of the dominant frequency at f_{k+1}, where $A_m[f_k] < A_m[f_{k+1}]$. In this case, f_{k+1} may be wrongly interpreted as the dominant harmonic frequency. In fact, the true interharmonic frequency in this case should be equal to f_k plus the 'frequency deviation' (Δf_k). Higher $A_m[f_{k+1}]$ will also introduce more amounts of deviation (Δf_k) from f_k.

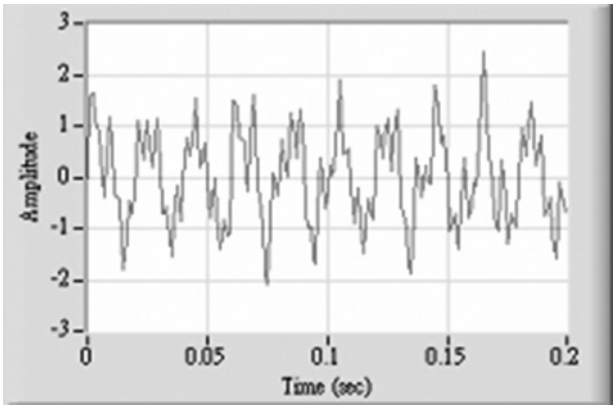

Fig. 3 *Waveform of s(t)*

If the length (N) of the sampled window for DFT is chosen correctly, no dispersed energy will exist and the spectrum can be thus achieved accurately. In Fig. 1*a*, it is noticed that the second stronger amplitude at f_{k+1} is found to be located at the right-hand side of the dominant component (f_k), i.e., $A_m[f_k] > A_m[f_{k+1}]$, in case of using overlong truncated-window length. On the contrary, in Fig. 1*b* the second stronger amplitude at f_k is located at the left side of the dominant component (f_{k+1}), i.e., $A_m[f_k] < A_m[f_{k+1}]$, the truncated-window length is insufficient for DFT analysis. From the basic theory, the window size should be appropriately selected to identify accurate interharmonics. The proposed MER approach is to collect all dispersed energy and thus determine a correct window length [36].

The flowchart of the proposed scheme is presented in Fig. 2, and it is illustrated as follows.

(i) The waveform $s(t)$ is sampled using $f_s = 1$ kHz, $N = 210$, i.e., $\Delta f = 5$ Hz. τ is set as 1.
(ii) Perform parallel DFT computation with $N = 190$–210 simultaneously.
(iii) Select $N = 200$ for initial process, and determine the number (m) of major harmonics/interharmonics.
(iv) If $A_m[f_{k+1}] > A_m[f_{k-1}]$, $N = N - 1$. Otherwise, go to the next step.
(v) If $A_m[f_{k+1}] < A_m[f_{k-1}]$, $N = N + 1$. Otherwise, go to the next step.
(vi) Check if $P_m^*[f_k]$ reaches the maximum point. If yes, the sampled number (N) is updated. $\Delta f'(=f_s/\mathrm{N})$ and $P_m^*[f_k]$ can be thus obtained. Accordingly, the true $A_m^*[f_k](=\sqrt{P_m^*[f_k]})$ and $f_k(=k\Delta f')$ can be found. Then, go to Step (8). Otherwise, go to the next step.
(vii) Repeat Steps (4)–(6) until the interharmonic is regained.
(viii) $m = m - 1$.
(ix) Check if $m = 0$. If yes, the iteration procedure stops, and all harmonics/interharmonics are found. Otherwise, go back to Step (3).

When the collected 'group power' $(P_m^*[f_k])$ from the proposed MER model reaches the maximum point during the convergent process, the actual adjacent interharmonic and similar frequency

IET Sci. Meas. Technol., 2016, Vol. 10, Iss. 2, pp. 92–99

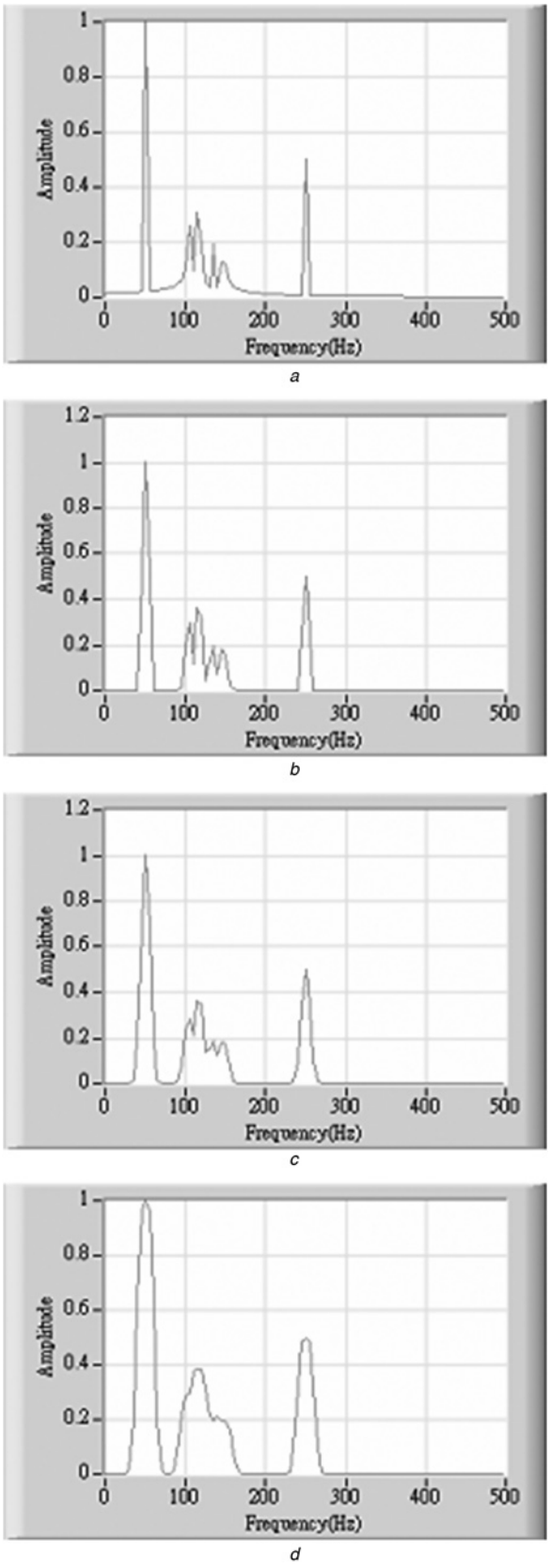

Fig. 4 *Spectrum analysis of s(t) using different windows*

a No added window
b Hanning window
c Four-Term Blackman–Harris window
d Flat top window

spectrum can be separated and identified accurately. At the time, the spectral leakage can be reduced to a satisfactory low level. For this purpose, multiple general-purpose microprocessors can allow DFT

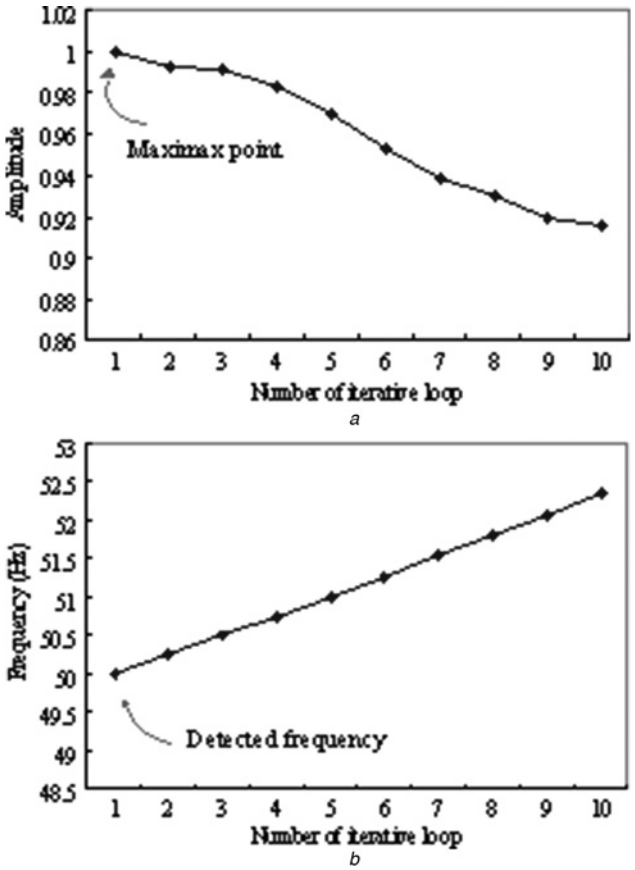

Fig. 5 *Fundamental frequency tracking curves at 50 Hz*

a Amplitude tracking
b Frequency tracking

to be performed simultaneously and independently, whose results are combined afterwards, upon completion.

4 Performance results

In Fig. 3, the waveform $s(t)$ that contains both harmonics and interharmonics is considered for test. This numerical example is cited from IEEE Interharmonic Task Force [34]. In addition to non-periodic characteristics in $s(t)$, the interharmonics are very close to some harmonics. However, please note that in this case $f_{i1} = 104$ Hz and $f_{i4} = 147$ Hz deviate from the second harmonic (100 Hz) and third harmonic (150 Hz), respectively.

$$\begin{aligned} s(t) = {} & a_1 \sin(2\pi \cdot f_1 \cdot t) + a_{i1} \sin(2\pi \cdot f_{i1} \cdot t) \\ & + a_{i2} \sin(2\pi \cdot f_{i2} \cdot t) + a_{i3} \sin(2\pi \cdot f_{i3} \cdot t) \\ & + a_{i4} \sin(2\pi \cdot f_{i4} \cdot t) + a_2 \sin(2\pi \cdot f_2 \cdot t) \end{aligned} \tag{11}$$

where $a_1 = 1.0$ and $a_2 = 0.5$ are the amplitudes of the fundamental and 5th harmonic, respectively, and their respective frequencies are $f_1 = 50$ Hz and $f_2 = 250$ Hz. The amplitudes of interharmonics are $a_{i1} = 0.3$, $a_{i2} = 0.4$, $a_{i3} = 0.2$, $a_{i4} = 0.2$, and their respective frequencies are $f_{i1} = 104$ Hz, $f_{i2} = 117$ Hz, $f_{i3} = 134$ Hz, $f_{i4} = 147$ Hz.

4.1 Spectrum analysis using DFT with window functions

Fig. 4*a* indicates the spectrum of $s(t)$ using DFT directly. The analysis results using Hanning window, Four-Term Blackman–Harris window, and Flat Top window are shown in Figs. 4*b–d*, respectively. It finds that Hanning and Four-Term Blackman–Harris windows can somehow improve the spectrum analysis slightly. However, spectrum result is even worse using Flat Top window. Clearly, none of spectrum analysis as above can carry out

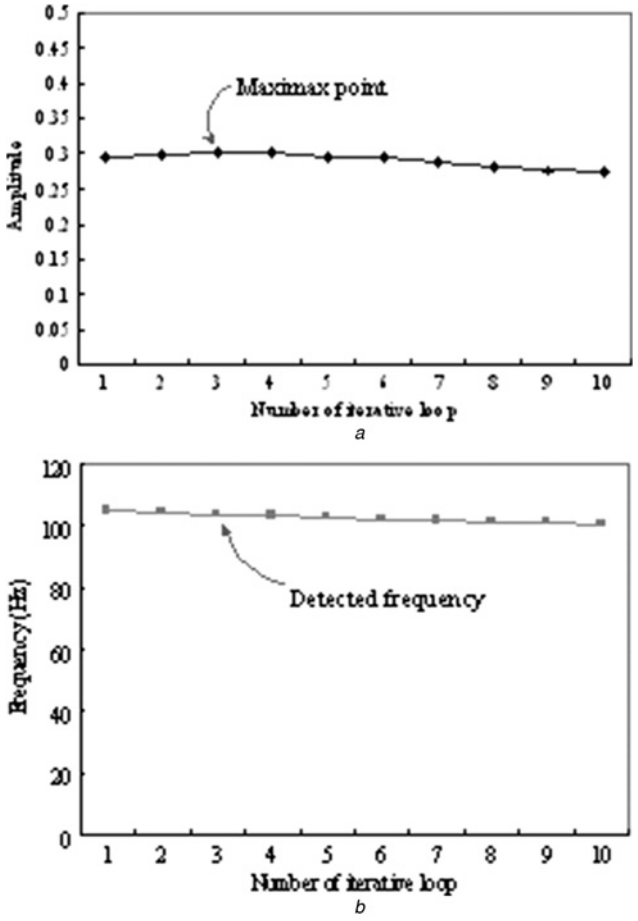

Fig. 6 *Interharmonic tracking curves at 104 Hz*

a Amplitude tracking
b Frequency tracking

Table 1 Parameters' values against iterative loop at 50 Hz

N	$m = 1,\ k = 10$					
	$P_m[f_{k-1}]$	$P_m[f_k]$	$P_m[f_{k+1}]$	$P_m^*[f_k]$	$A_m^*[f_k]$	f_k
200	0.00046	1	0.00054	1.001	1.0[a]	50[a]
199	0.004	0.98	0.0028	0.987	0.993	50.25
198	0.014	0.96	0.008	0.982	0.991	50.51
197	0.032	0.92	0.015	0.967	0.983	50.76
196	0.06	0.86	0.022	0.942	0.97	51.02
195	0.1	0.78	0.027	0.907	0.952	51.28
194	0.16	0.69	0.03	0.88	0.938	51.55
193	0.22	0.61	0.033	0.863	0.93	51.81
192	0.29	0.52	0.032	0.842	0.92	52.08
191	0.38	0.43	0.029	0.839	0.916	52.36

[a]denotes the solution achieved

adjacent interharmonics measurement accurately. As can be seen, all interharmonic frequencies are unable to be distinguished, and also the spectral leakage still spreads seriously.

4.2 Spectrum analysis using MER model

In this section, the performance results using the proposed MER model are presented to demonstrate how the model identifies the interharmonics that are close to fundamental or harmonics. There are six cases, i.e., 50, 104, 117, 134, 147, and 250 Hz evaluated and discussed, respectively. The 'group power' ($P_m^*[f_k]$) in (9) is primarily used to evaluate the performance process.

Table 2 Parameters' values against iterative loop at 104 Hz

N	$m = 2,\ k = 21$					
	$P_m[f_{k-1}]$	$P_m[f_k]$	$P_m[f_{k+1}]$	$P_m^*[f_k]$	$A_m^*[f_k]$	f_k
200	0.01	0.068	0.0089	0.087	0.294	105
201	0.0045	0.077	0.0084	0.090	0.299	104.48
202	0.0016	0.083	0.0067	0.091	0.302[a]	103.96*
203	0.0014	0.083	0.0057	0.090	0.3	103.45
204	0.0028	0.077	0.0072	0.087	0.295	102.94
205	0.0049	0.069	0.012	0.086	0.293	102.44
206	0.0068	0.057	0.019	0.083	0.288	101.94
207	0.0077	0.044	0.028	0.080	0.282	101.45
208	0.0071	0.03	0.039	0.076	0.276	100.96
209	0.0051	0.017	0.053	0.075	0.274	100.48

[a]denotes the solution achieved

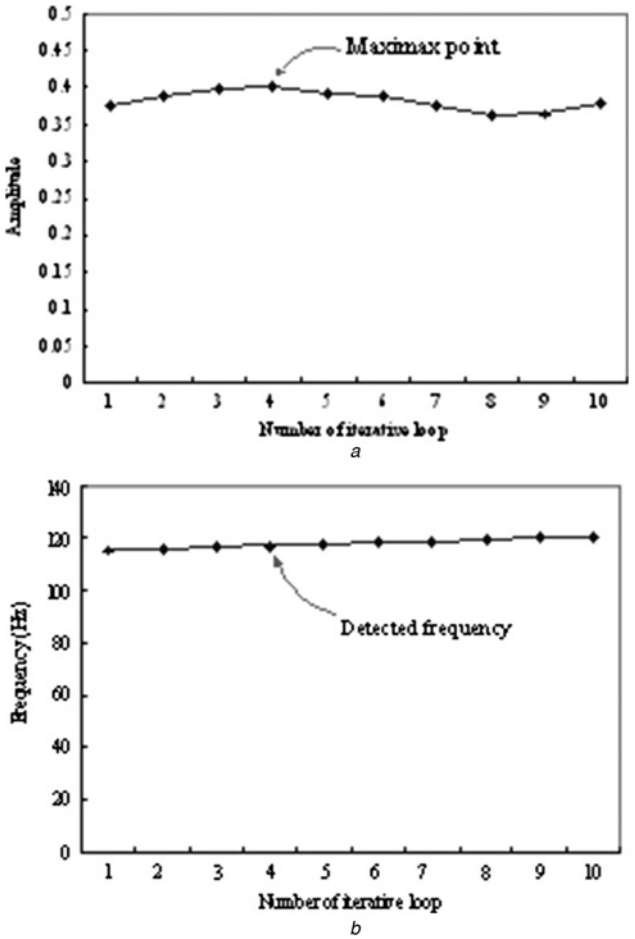

Fig. 7 *Interharmonic tracking curves at 117 Hz*

a Amplitude tracking curve
b Frequency tracking curve

4.2.1 Case 1: 50 Hz fundamental frequency tracking: From Fig. 5*a*, it is seen that the amplitude of 50 Hz fundamental frequency is found as 1.0 when the retrieved amplitude reaches the maximum point at the first iteration loop. Consequently, the detected frequency is determined as 50 Hz, shown in Fig. 6*b*. The model's parameter values against iterative loop are listed in Table 1.

4.2.2 Case 2: 104 Hz interharmonic tracking: In Fig. 6*a*, initially the amplitude of 104 Hz interharmonic is found as 0.294. The retrieved amplitude soon reaches the maximum point at the third iteration loop where the amplitude value is 0.30. As a result, the detected frequency is determined as 103.96 Hz, shown in

IET Sci. Meas. Technol., 2016, Vol. 10, Iss. 2, pp. 92–99

Table 3 Parameters' values against iterative loop at 117 Hz

N	$m = 3,\ k = 23$					
	$P_m[f_{k-1}]$	$P_m[f_k]$	$P_m[f_{k+1}]$	$P_m^*[f_k]$	$A_m^*[f_k]$	f_k
200	0.0089	0.097	0.035	0.141	0.375	115
199	0.0074	0.13	0.016	0.153	0.391	115.57
198	0.0047	0.15	0.0046	0.159	0.399	116.16
197	0.0024	0.16	0.00026	0.163	0.4[a]	116.75[a]
196	0.0031	0.15	0.0006	0.154	0.392	117.3
195	0.01	0.14	0.0026	0.153	0.391	117.9
194	0.026	0.11	0.0041	0.140	0.374	118.5
193	0.052	0.076	0.0041	0.132	0.363	119.17
192	0.084	0.046	0.003	0.133	0.365	119.79
191	0.12	0.023	0.0015	0.145	0.38	120.41

[a]denotes the solution achieved

Table 4 Parameters' values against iterative loop at 134 Hz

N	$m = 4,\ k = 27$					
	$P_m[f_{k-1}]$	$P_m[f_k]$	$P_m[f_{k+1}]$	$P_m^*[f_k]$	$A_m^*[f_k]$	f_k
200	0.0014	0.039	0.0014	0.042	0.204	135
201	0.00081	0.052	0.00031	0.053	0.207[a]	134.32[a]
202	0.0013	0.04	0.00042	0.042	0.204	133.66
203	0.0017	0.034	0.0029	0.039	0.196	133
204	0.0014	0.025	0.0082	0.035	0.186	132.35
205	0.00097	0.016	0.015	0.032	0.179	131.71
206	0.0013	0.0091	0.023	0.033	0.183	131.07
207	0.0026	0.0046	0.03	0.037	0.193	130.43
208	0.0045	0.0023	0.035	0.042	0.204	129.8
209	0.0064	0.0019	0.037	0.045	0.21	129.19

[a]denotes the solution achieved

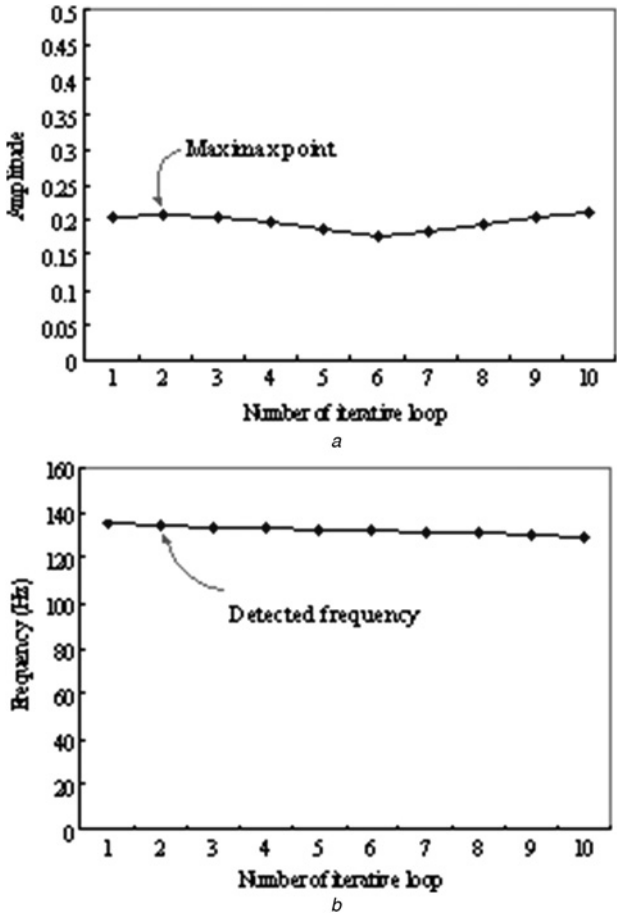

Fig. 8 *Interharmonic tracking curves at 134 Hz*

a Amplitude tracking curve
b Frequency tracking curve

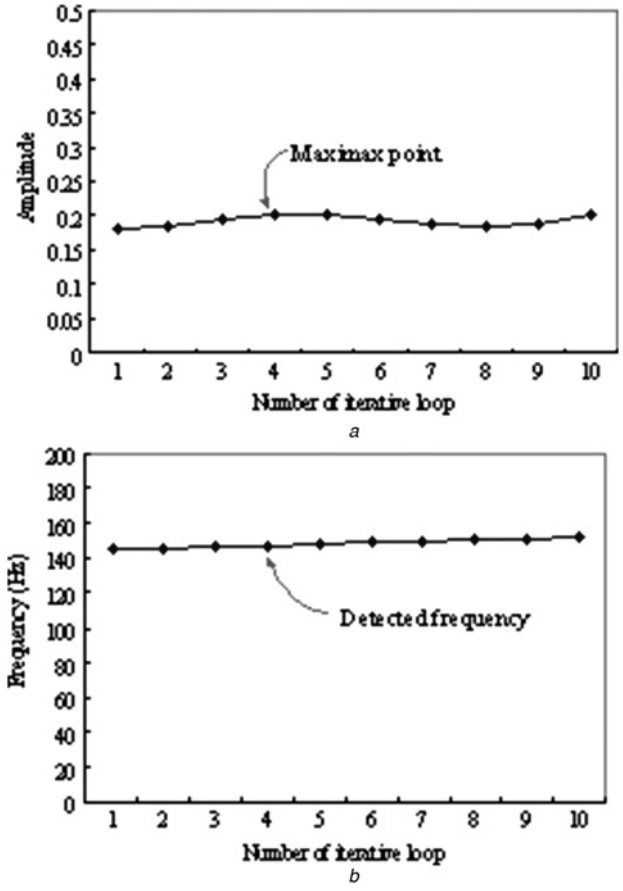

Fig. 9 *Interharmonic tracking curves at 147 Hz*

a Amplitude tracking curve
b Frequency tracking curve

Fig. 6*b*. The model's parameter values against iterative loop are listed in Table 2.

4.2.3 Case 3: 117 Hz interharmonic tracking: From Fig. 7*a*, the amplitude of 117 Hz interharmonic is found as 0.38 at the first stage. The retrieved amplitude approaches the maximum point at the fourth iteration loop where the amplitude value is 0.40. Accordingly, the detected frequency is determined as 116.8 Hz, shown in Fig. 7*b*. The model's parameter values against iterative loop are listed in Table 3.

4.2.4 Case 4: 134 Hz interharmonic tracking: From Fig. 8*a*, the amplitude of 134 Hz interharmonic is obtained as 0.20 at the first stage. The retrieved amplitude approaches the maximum point at the second iteration loop where the amplitude value is 0.21. Therefore, the detected frequency is determined as 134.3 Hz, shown in Fig. 8*b*. The model's parameter values against iterative loop are listed in Table 4.

4.2.5 Case 5: 147 Hz interharmonic tracking: In Fig. 9*a*, initially the amplitude of 147 Hz interharmonic is found as 0.18. The retrieved amplitude reaches to the maximum point at the fourth iteration loop where the amplitude value is 0.20. Consequently, the detected frequency is determined as 147.2 Hz, shown in Fig. 9*b*. The model's parameter values against iterative loop are listed in Table 5.

4.2.6 Case 6: 250 Hz harmonic tracking: From Fig. 10*a*, the amplitude of 250 Hz harmonic frequency is found as 0.5 where

Table 5 Parameters' values against iterative loop at 147 Hz

N	$m = 5,\ k = 29$					
	$P_m[f_{k-1}]$	$P_m[f_k]$	$P_m[f_{k+1}]$	$P_m^*[f_k]$	$A_m^*[f_k]$	f_k
200	0.0014	0.016	0.015	0.0324	0.18	145
199	0.0025	0.025	0.0069	0.0344	0.185	145.7
198	0.0031	0.033	0.0021	0.0382	0.195	146.6
197	0.0028	0.038	0.00068	0.0415	0.204[a]	147.2[a]
196	0.0029	0.037	0.0014	0.0413	0.203	147.96
195	0.0053	0.031	0.0025	0.0388	0.197	148.72
194	0.011	0.021	0.003	0.035	0.187	149.48
193	0.02	0.012	0.0025	0.0345	0.186	150.26
192	0.03	0.0049	0.0016	0.0365	0.19	151.04
191	0.038	0.0015	0.00082	0.040	0.2	151.83

[a]denotes the solution achieved

Table 6 Parameters' values against iterative loop at 250 Hz

N	$m = 6,\ k = 50$					
	$P_m[f_{k-1}]$	$P_m[f_k]$	$P_m[f_{k+1}]$	$P_m^*[f_k]$	$A_m^*[f_k]$	f_k
200	4.9×10^{-5}	0.25	4×10^{-5}	0.25	0.5[a]	250[a]
201	0.007	0.2	0.024	0.23	0.48	248.76
202	0.0099	0.097	0.11	0.22	0.47	247.52
203	0.004	0.022	0.2	0.23	0.48	246.31
204	0.00014	0.00013	0.24	0.24	0.49	245.1
205	0.0011	0.0054	0.19	0.20	0.45	243.90
206	0.0024	0.0083	0.092	0.1	0.32	242.72
207	0.0015	0.0037	0.021	0.03	0.17	241.55
208	0.00019	0.00018	0.00017	5.4×10^{-4}	0.02	240.38
209	0.0008	0.0019	0.0069	9.6×10^{-3}	0.1	239.23

[a]denotes the solution achieved

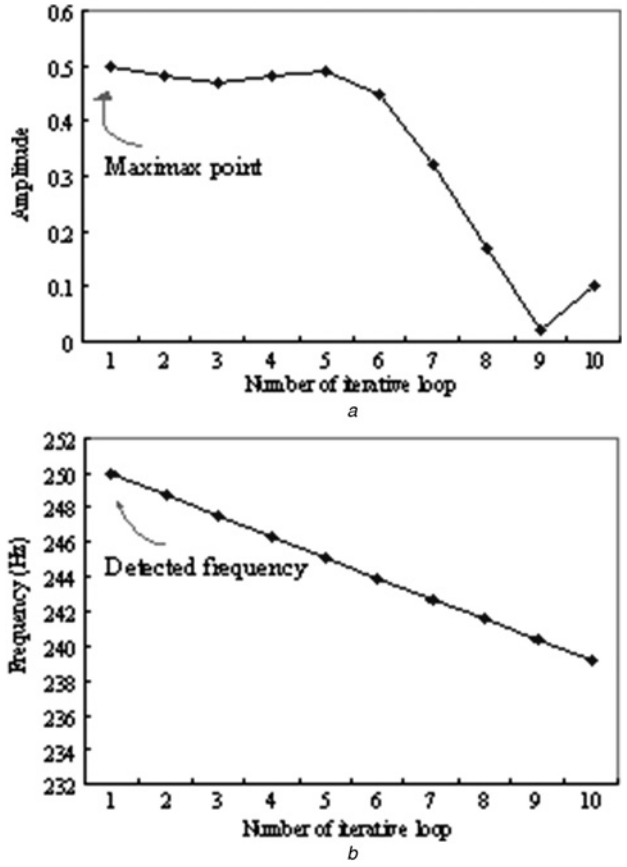

Fig. 10 *Harmonic tracking curves at 250 Hz*

a Amplitude tracking curve
b Frequency tracking curve

the retrieved amplitude reaches the maximum point at the first iteration loop. Therefore, the detected frequency is determined as 250 Hz, shown in Fig. 10*b*. The model's parameter values against iterative loop are listed in Table 6.

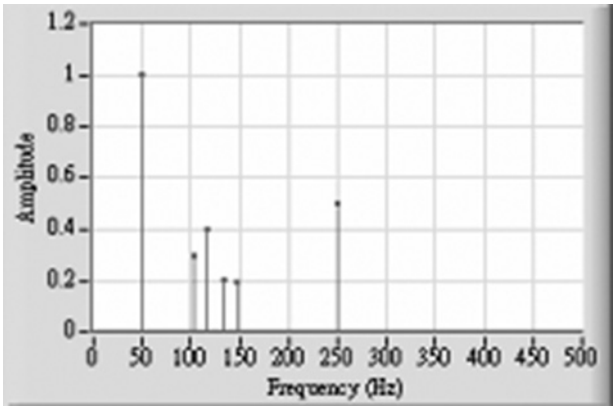

Fig. 11 *Spectrum of s(t) using MER*

In conclusion of above results (Tables 1 to 6), the spectrum of $s(t)$ using MER is shown in Fig. 11. Obviously, each interharmonic is distinguished and identified accurately without spectrum leakage. It is clear that the proposed model presents better performance than traditional DFT or windowed DFT. However, the spectrum analysis using MER has no difference with DFT in fundamental and harmonic components, e.g., 50 and 250 Hz, because both of them can achieve an accurate measurement in this case. The comparison of result between DFT and MER is summed up in Table 7.

4.3 Discussion for selection of group bandwidth (τ)

Spectrum analysis using DFT may cause spectral leakage if the waveform contains interharmonics. In such a situation, the power of the harmonic at f_k may disperse over a frequency band. Normally, the larger group bandwidth (τ) may restore all leakages and thus regain the actual amplitude/frequency. However, with a large bandwidth the 'group power' may cover some harmonic contents at distant frequencies. For this reason, the group bandwidth (τ) should be chosen as large as possible but small enough to avoid the overlap between two neighbouring harmonic

Table 7 Result comparison between DFT and MER

Methods	Real values					
	$f_1 = 50$ (Hz) $a_1 = 1.0$	$f_{i1} = 104$ (Hz) $a_{i1} = 0.3$	$f_{i2} = 117$ (Hz) $a_{i2} = 0.4$	$f_{i3} = 134$ (Hz) $a_{i3} = 0.2$	$f_{i4} = 147$ (Hz) $a_{i4} = 0.2$	$f_2 = 250$ (Hz) $a_2 = 0.5$
DFT	$f_1 = 50$ (Hz) $a_1 = 1.0$	$f_{i1} = 105$ $a_{i1} = 0.29$	$f_{i2} = 115$ $a_{i2} = 0.38$	$f_{i3} = 135$ $a_{i3} = 0.20$	$f_{i4} = 145$ $a_{i4} = 0.18$	$f_2 = 250$ (Hz) $a_2 = 0.5$
MER	$f_1 = 50$ (Hz) $a_1 = 1.0$	$f_{i1} = 104$ $a_{i1} = 0.30$	$f_{i2} = 116.8$ $a_{i2} = 0.40$	$f_{i3} = 134.3$ $a_{i3} = 0.21$	$f_{i4} = 147.2$ $a_{i4} = 0.20$	$f_2 = 250$ (Hz) $a_2 = 0.5$

IET Sci. Meas. Technol., 2016, Vol. 10, Iss. 2, pp. 92–99

groups. In this study, interharmonics are very close to fundamental or harmonics, so that τ is chosen as 1 with $\Delta f = 5$ Hz to exclude possible dispersed power interaction between each other.

5 Conclusions

A number of related algorithms focused on the impact or measurement of harmonics/interharmonics in power systems have been reported in the literature. However, it is still unsolved for the identification of those interharmonics close to harmonics or fundamental. In the proposed scheme, both amplitude and frequency of interharmonics can be obtained accurately by collecting the maximum energy dispersed from spectrum leakage, where only several iteration loops are required. $\Delta f = 5$ Hz recommended by IEC is selected for the trade-off between the sampling time and measurement accuracy, and therefore the sampling time (=200 ms) is quite reasonable. From the performance results, it can be seen that the proposed MER method is superior to the traditional DFT. For industrial applications, no extended memory is needed in general computers or microprocessors. Accordingly, it can be easily applied to DFT-based instruments due to its simple mathematics basis of DFT.

6 References

1 Eastham, J.F., Cox, T., Proverbs, J.: 'Application of planar modular windings to linear induction motors by harmonic cancellation', *IET Electr. Power Appl.*, 2010, **4**, (3), pp. 140–148
2 Zhao, W.X., Cheng, M., Chau, K.T., *et al.*: 'Control and operation of fault-tolerant flux-switching permanent-magnet motor drive with second harmonic current injection', *IET Electr. Power Appl.*, 2012, **6**, (9), pp. 707–715
3 Gallo, D., Langella, R., Testa, A.: 'Interharmonics, Part 2: aspects related to measurement and limits'. Sixth Int. Workshop on Power Definitions and Measurements under Non-Sinusoidal Conditions, Milano, 13–15 October 2003, pp. 174–181
4 Masoum, M.A.S., Moses, P.S.: 'Impact of balanced and unbalanced direct current bias on harmonic distortion generated by asymmetric three-phase three-leg transformers', *IET Electr. Power Appl.*, 2010, **4**, (7), pp. 507–515
5 Karimi-Ghartemani, M., Reza Iravani, M.: 'Measurement of harmonics/inter-harmonics of time-varying frequency', *IEEE Trans. Power Deliv.*, 2005, **20**, (1), pp. 23–31
6 Lin, H.C.: 'Fast tracking of time-varying power system frequency and harmonics using iterative-loop approaching algorithm', *IEEE Trans. Ind. Electron.*, 2007, **54**, (2), pp. 974–983
7 Aghazadeh, R., Lesani, H., Sanaye-Pasand, M., *et al.*: 'New technique for frequency and amplitude estimation of power system signals', *IEE Proc. Gener. Transm. Distrib.*, 2005, **152**, (3), pp. 435–440
8 Li, C., Xu, W., Tayjasanant, T.: 'Interharmonics: basic concepts and techniques for their detection and measurement', *Electr. Power Syst. Res.*, 2003, **66**, (1), pp. 39–48
9 Tayjasanant, T., Wang, W., Li, C., *et al.*: 'Interharmonic-flicker curves', *IEEE Trans. Power Deliv.*, 2005, **20**, (2), pp. 1017–1024
10 Lobos, T., Kozina, T., Koglin, H.-J.: 'Power system harmonics estimation using linear least squares method and SVD', *IEE Proc. Gener. Transm. Distrib.*, 2001, **148**, (6), pp. 567–572
11 Lin, H.C.: 'Intelligent neural network based adaptive power line conditioner for real-time harmonics filtering', *IEE Proc. Gener. Transm. Distrib.*, 2004, **151**, (5), pp. 561–567
12 Saiz, V.M.M., Guadalupe, J.B.: 'Application of Kalman filtering for continuous real-time tracking of power system harmonics', *IEE Proc. Gener. Transm. Distrib.*, 1998, **144**, (1), pp. 13–20
13 Dash, P.K., Panda, S.K., Mishra, B., *et al.*: 'Fast estimation of voltage and current phasors in power networks using an adaptive neural network', *IEEE Trans. Power Syst.*, 1997, **12**, (4), pp. 1494–1499
14 Caijun, Q., Xiaohai, W.: 'Interharmonics estimation based on interpolation FFT algorithm', *Trans. China Electrotech. Soc.*, 2003, **18**, (I1), pp. 92–95
15 Testa, A., Gallo, D., Langella, R.: 'On the processing of harmonics and interharmonics: using hanning window in standard framework', *IEEE Trans. Power Deliv.*, 2006, **21**, (1), pp. 538–539
16 Qian, H., Zhao, R., Chen, T.: 'Interharmonics analysis based on interpolating windowed FFT algorithm', *IEEE Trans. Power Deliv.*, 2007, **22**, (2), pp. 1064–1069
17 Testa, A., Gallo, D., Langella, R.: 'On the processing of harmonics and interharmonics: using Hanning window in standard framework', *IEEE Trans. Power Deliv.*, 2004, **19**, (1), pp. 28–34
18 Thomas, D.W.P., Woolfson, M.S.: 'Evaluation of frequency tracking methods', *IEEE Trans. Power Deliv.*, 2001, **16**, (3), pp. 367–371
19 Agrez, D.: 'Weighted multipoint interpolated DFT to improve amplitude estimation of multifrequency signal', *IEEE Trans. Instrum. Meas.*, 2002, **51**, (2), pp. 287–292
20 Lin, H.C.: 'Intelligent neural network based fast power system harmonic detection', *IEEE Trans. Ind. Electron.*, 2007, **54**, (1), pp. 43–52
21 Dehini, R., Bassou, A., Ferdi, B.: 'The harmonics detection method based on neural network applied to harmonics compensation', *Int. J. Eng. Sci. Technol.*, 2010, **2**, (5), pp. 258–267
22 Chang, G.W., Chen, S.-K., Su, H.-J., *et al.*: 'Accurate assessment of harmonic and interharmonic currents generated by VSI-fed drives under unbalanced supply voltages', *IEEE Trans. Power Deliv.*, 2011, **26**, (2), pp. 1083–1091
23 Nassif, A.B., Yong, J., Mazin, H., *et al.*: 'An impedance-based approach for identifying interharmonic sources', *IEEE Trans. Power Deliv.*, 2011, **26**, (1), pp. 333–340
24 Hidalgo, R.M., Fernandez, J.G., Rivera, R.R., *et al.*: 'A simple adjustable window algorithm to improve FFT measurements', *IEEE Trans. Instrum. Meas.*, 2002, **51**, (01), pp. 31–36
25 Zhu, T.X.: 'Exact harmonics/interharmonics calculation using adaptive window width', *IEEE Trans. Power Deliv.*, 2007, **22**, (4), pp. 2279–2288
26 Chang, G.W., Chen, C.-I.: 'An accurate time-domain procedure for harmonics and interharmonics detection', *IEEE Trans. Power Deliv.*, 2010, **25**, (3), pp. 1787–1795
27 Gu, I.Y.-H., Bollen, M.H.J.: 'Estimating interharmonics by using sliding-window ESPRIT', *IEEE Trans. Power Deliv.*, 2008, **23**, (1), pp. 13–23
28 Jain, S.K., Singh, S.N.: 'Exact model order ESPRIT technique for harmonics and interharmonics estimation', *IEEE Trans. Instrum. Meas.*, 2012, **61**, (7), pp. 1915–1923
29 He, C., Shu, Q.: 'Separation and analyzing of harmonics and inter-harmonics based on single channel independent component analysis', *Int. Trans. Electr. Energy Syst.*, 2015, **25**, pp. 169–179
30 Jin, H., Honggeng, Y.: 'Harmonics and interharmonics separate-detection method based on estimation of leakage values caused by interharmonics', *Trans. China Electrotech. Soc.*, 2011, **26**, (1), pp. 183–191
31 Agrez, D.: 'Weighted multipoint interpolated DFT to improve amplitude estimation of multifrequency signal', *IEEE Trans. Instrum. Meas.*, 2002, **51**, (2), pp. 287–292
32 Wu, R.-C., Tai, C.C.: 'Analysis of the exponential signal by the interpolated DFT algorithm', *IEEE Trans. Instrum. Meas.*, 2010, **59**, (12), pp. 3306–3317
33 IEC 61000-4-7: 'Testing and measurement techniques: harmonics and inter-harmonics: general guide on harmonics and inter-harmonics measurements and instrumentation for power supply systems and equipment connected thereto', 2002
34 Interharmonics in power systems: 'IEEE interharmonic task force', Cigré 36.05/CIRED 2 CC02 voltage quality working group
35 Ramirez, A.: 'The modified harmonic domain: interharmonics', *IEEE Trans. Power Deliv.*, 2011, **26**, (1), pp. 235–241
36 Lin, H.C.: 'Power harmonics and interharmonics measurement using recursive group-harmonic power minimizing algorithm', *IEEE Trans. Ind. Electron.*, 2012, **59**, (2), pp. 1184–1193
37 Hajibeigy, M., Farsadi, M., Nazarpour, D., *et al.*: 'Harmonic suppression in HVDC system using a modified control method for hybrid active DC filter', *Eur. Trans. Electr. Power*, 2012, **22**, (3), pp. 294–307
38 Sadinezhad, I., Agelidis, V.G.: 'Real-time power system phasors and harmonics estimation using a new decoupled recursive-least-squares technique for DSP implementation', *IEEE Trans. Ind. Electron.*, 2013, **60**, (6), pp. 2295–2308
39 Jain, S.K., Singh, S.N.: 'Fast harmonic estimation of stationary and time-varying signals using EA-AWNN', *IEEE Trans. Instrum. Meas.*, 2013, **62**, (2), pp. 335–343
40 Lin, H.C.: 'Accurate harmonic/inter-harmonic estimation using DFT-based group-harmonics energy diffusion algorithm', *Can. J. Electr. Comput. Eng.*, 2014, **36**, (4), pp. 158–171
41 Lin, H.C.: 'Sources, effects and modelling of interharmonics', *Math. Probl. Eng.*, 2014, **2014**, pp. 1–10
42 Chen, C.I., Chen, Y.C., Chang, Y.R., *et al.*: 'An accurate solution procedure for calculation of voltage flicker components', *IEEE Trans. Ind. Electron.*, 2014, **61**, (5), pp. 2370–2377
43 Chen, C.-I., Chen, Y.-C.: 'Comparative study of harmonic and interharmonic estimation methods for stationary and time-varying signals', *IEEE Trans. Ind. Electron.*, 2014, **61**, (1), pp. 397–404
44 Chakir, M., Kamwa, I., Le Huy, H.: 'Extended C37.118.1 PMU algorithms for joint tracking of fundamental and harmonic phasors in stressed power systems and microgrids', *IEEE Trans. Power Deliv.*, 2014, **29**, (3), pp. 1465–1480
45 Valtierra-Rodriguez, M., de Jesus Romero-Troncoso, R., Osornio-Rios, R.A., *et al.*: 'Detection and classification of single and combined power quality disturbances using neural networks', *IEEE Trans. Ind. Electron.*, 2014, **61**, (5), pp. 2473–2482
46 Jain, S.K., Singh, S.N.: 'Low-order dominant harmonic estimation using adaptive wavelet neural network', *IEEE Trans. Ind. Electron.*, 2014, **61**, (1), pp. 428–435
47 Testa, A., Akram, M.F., Burch, R., *et al.*: 'Interharmonics: theory and modeling', *IEEE Trans. Power Deliv.*, 2007, **22**, (4), pp. 2335–2348
48 Oppenheim, A.V., Schafer, R.W.: 'Discrete-time signal processing' (Prentice–Hall, 1989)
49 Press, W.H., Flannery, B.P., Teukolsky, S.A., *et al.*: 'Numerical recipes-the art of scientific computing' (Cambridge University, Cambridge, 1986), pp. 420–429